

Received: 2019.08.01
Accepted: 2019.09.30
Published: 2019.10.25

A Pilot Study of Third-Generation Dual-Source Computed Tomography for the Assessment of Global Dynamic Changes in Left Ventricular Structure and Function in a Porcine Model of Acute Myocardial Infarction

Authors' Contribution:

Study Design A
Data Collection B
Statistical Analysis C
Data Interpretation D
Manuscript Preparation E
Literature Search F
Funds Collection G

CEG 1,2 **Wenjia Li**
A 2 **Liang Lyu**
B 2 **Weixin Yang**
B 3 **Rongshun Zhang**
F 2 **Gang Wang**
D 2 **Dong Fan**
C 2 **Wei Song**
B 2 **Junkun Yin**
B 2 **Jiangmao Yang**
B 2 **Wei Li**
B 4 **Liling Chen**
A 5 **Tianyou Luo**

1 Chongqing Medical University, Chongqing, P.R. China
2 Department of Radiology, First People's Hospital of Yunnan, Kunming, Yunnan, P.R. China
3 Department of Radiology, Third People's Hospital of Yunnan, Kunming, Yunnan, P.R. China
4 Kunming Medical University, Kunming, Yunnan, P.R. China
5 Department of Radiology, First Affiliated Hospital of Chongqing Medical University, Chongqing, P.R. China

Corresponding Author: Tianyou Luo, e-mail: ltycqfs@126.com

Source of support: This study was funded by the Health and Technology Program of Yunnan (Grant number: 2014NS261)

Background: First-generation and second-generation dual-source computed tomography (DSCT) are useful for analyzing left ventricle (LV) structure and function. This pilot study aimed to investigate the feasibility and role of third-generation DSCT for the evaluation of dynamic changes in LV structural and functional characteristics in a Diannan small-ear pig model of acute myocardial infarction (AMI).



Material/Methods: The model of AMI was established by balloon occlusion of the distal third of the left anterior descending (LAD) coronary artery in 14 Diannan small-eared pigs. Third-generation DSCT was performed to observe dynamic changes in LV structure and function before and after AMI was induced, with a follow-up period of 30 days.

Results: The mean structural measurements at baseline included interventricular septum thickness (8.50 ± 0.90 mm), LV anterior wall thickness (8.40 ± 1.30 mm), LV posterior wall thickness (7.80 ± 1.20 mm), LV end-diastolic dimension (LVEDD) (45.00 ± 4.90 mm), and LV end-systolic dimension (LVESD) (25.90 ± 4.10 mm). The mean functional measurements at baseline included the LV end-diastolic volume (LVEDV) (74.62 ± 13.54 ml), LV end-systolic volume (LVESV) (23.06 ± 7.46 ml), LV ejection fraction (LVEF) ($69.29 \pm 6.83\%$), LV mass (86.35 ± 14.02 g), stroke volume (SV) (51.56 ± 9.77 ml), and cardiac output (CO) (4.22 ± 2.14 l/min). Trends of time-dependent changes were observed for LVESV, LVEF, SV, and CO, but not for LVEDV or LV mass.

Conclusions: Third-generation DSCT was validated as a tool for assessing dynamic changes in LV global function in a porcine model of AMI.

MeSH Keywords: **Coronary Artery Disease • Multidetector Computed Tomography • Swine • Ventricular Function, Left**

Full-text PDF: <https://www.medscimonit.com/abstract/index/idArt/919122>

 2957  1  5  32



Background

Acute myocardial infarction (AMI) is a serious clinical consequence of coronary heart disease (CHD) due to atherosclerosis and is a major cause of morbidity and mortality worldwide [1,2]. Non-invasive imaging methods have become increasingly used for the diagnosis and evaluation of AMI and continue to be studied and refined [3,4]. Although magnetic resonance imaging (MRI) is established as the standard for non-invasive imaging examination of cardiac structure and function [5], cardiac computed tomography (CT) is also commonly used in clinical practice because it is easy to perform, and is both time-saving and cost-saving when compared with cardiac MRI [5,6]. The use of cardiac CT, or multidetector computed tomography (MDCT), allows data to be obtained for cardiac structure and function within a single heartbeat [6]. Also, CT is the examination of choice for patients with contraindications for MRI, including for patients with metal implants or patients with severe claustrophobia [7]. In 2005, dual-source computed tomography (DSCT) was developed and showed efficacy for the evaluation of coronary artery stenosis [8,9]. The application of retrospective gating in DSCT permits the evaluation of the status of cardiac function and myocardial perfusion, which currently means that CT scanning is an alternative imaging procedure to MRI for clinical evaluation of patients with CHD [10–13].

In 2015, advances in imaging resulted in the introduction of third-generation DSCT that offered the availability of a complete evaluation of the morphology of the left ventricle (LV) and global cardiac function [14,15]. The associated reduction in the use of contrast agents and the reduction in radiation dose further expanded the clinical application of CT cardiac imaging [16]. Recent meta-analysis data showed that cardiac CT provided an accurate assessment of global LV function and LV wall motion deficits, but the limits of agreement compared with cardiac MRI were moderately wide [15]. Therefore, cardiac CT provides a one-stop non-invasive imaging technique to evaluate both the severity of coronary artery stenosis and the status of cardiac function.

Preclinical studies in animal models of AMI are important for accelerating the application of translational research findings clinically in patients with CHD. Because the anatomy of the pig is similar to that of humans, including the anatomy of the coronary arteries, porcine models of AMI have been developed [17]. Compared with echocardiography and MRI, cardiac CT is less time-consuming and less influenced by the acoustic window and the breathing and heart rate of experimental animals. Although various non-invasive imaging techniques such as echocardiography, radionuclide myocardial imaging, CT, and MRI have been applied in animal studies of cardiovascular diseases [18–20], studies focusing on baseline cardiac data in pig models are rare [20–22]. Chinese miniature pigs are commonly

used in research as animal models of human cardiovascular disease, but the baseline structural and functional characteristics of the LV measured by DSCT have not been fully evaluated. Dynamic changes in LV function following AMI are closely correlated with clinical risk category and clinical prognosis and are important areas to study in animal models.

Therefore, this pilot study aimed to investigate the feasibility and role of third-generation DSCT for the evaluation of dynamic changes in LV structural and functional characteristics in a Diannan small-ear pig model of AMI. The findings from this study may provide essential basic data and reference values for CT evaluation in preclinical studies of AMI in miniature pigs.

Material and Methods

Animal groups and preparation

All animal experiments were approved by the Animal Committee of Kunming Medical University (Approval Number: Kmmu2019042), and the study complied with local and national laboratory animal management regulations. Fourteen healthy adult Diannan small-eared pigs of either sex with an average weight of 39.57 ± 5.61 kg were used in this study. The animals were randomized into a normal control group ($n=6$) or an experimental group in the porcine model of acute myocardial infarction (AMI) ($n=8$). All animals were fasted for 12 hours and prevented from drinking water for 4 hours before the procedure. Anesthesia was induced with xylazine hydrochloride (0.1 ml/kg) and ketamine hydrochloride (5 mg/kg) and maintained with 3.0% sodium pentobarbital via a 24G trocar placed in an ear vein. No additional medication was applied to reduce the respiratory rate or heart rate.

The Diannan small-ear pig model of acute myocardial infarction (AMI) and coronary artery angiography

In the eight animals in the experimental group, AMI was induced using a closed-chest model after baseline examination with third-generation dual-source computed tomography (DSCT). For this purpose, a 6F guide wire (FMD Co, Ltd, Minato-ku, Tokyo, Japan) was inserted in the right femoral artery. A Launcher 6F guide catheter (Medtronic, Danvers, MA, USA) was placed in the left main coronary artery trunk, and coronary angiography was performed to visualize the anatomic characteristics of the left coronary arteries. A detachable Sprinter Legend balloon (Medtronic, Minneapolis, MN, USA) with a diameter of 2.0–2.5 mm was used to induce occlusion of the distal third of the left anterior descending (LAD) coronary artery, distal to the second diagonal artery. Repeat coronary angiography showed complete arterial occlusion (Figure 1). The entire process was performed with the animals monitored

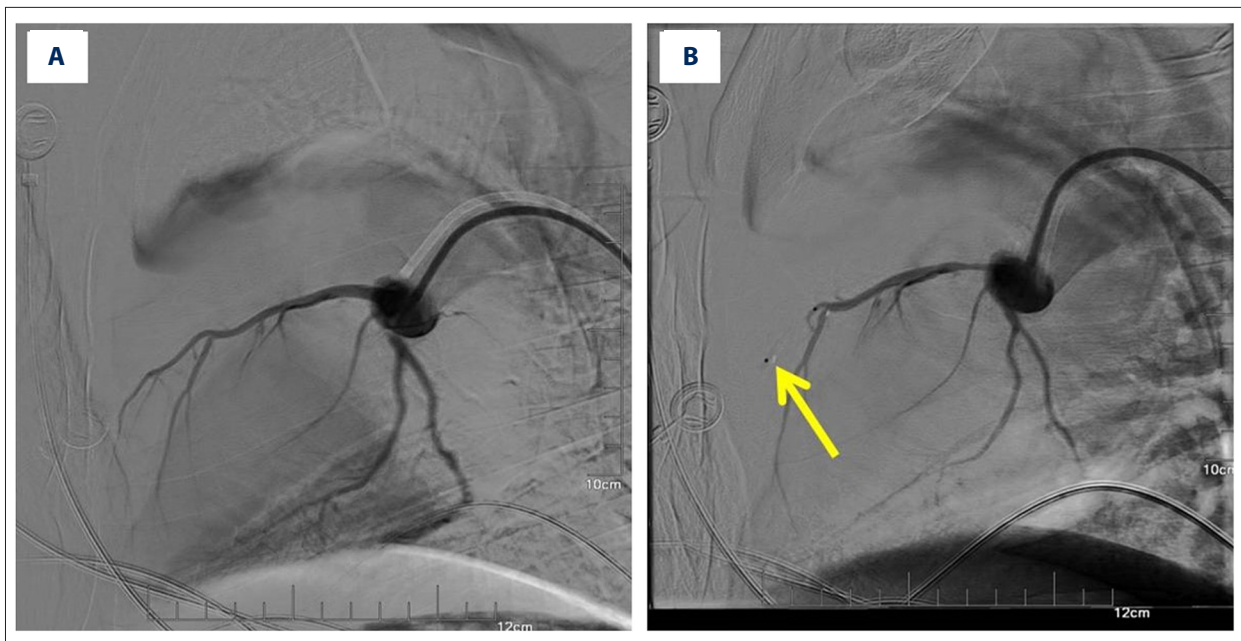


Figure 1. Representative images of the induction of acute myocardial infarction (AMI) in the porcine closed-chest model. (A) Coronary angiography was performed to visualize the anatomy of the left coronary artery before occlusion. (B) A detachable balloon was used to occlude the distal third of the left anterior descending coronary artery in the same projection shown in (A).

by electrocardiography (ECG). To prevent dehydration, all animals received a constant infusion of normal saline.

The third-generation dual-source computed tomography (DSCT) imaging protocol

Third-generation DSCT scanning was performed with a SOMATOM Force dual-source CT scanner (Siemens Healthcare, Forchheim, Germany) before the procedure, and at 1 hour, 3 hours, 6 hours, 12 hours, 24 hours, 2 days, 3 days, 7 days, and 30 days after AMI induction. A standardized examination protocol was applied, with 0.6×128 slices collimated for both detectors, a tube rotation time of 0.25 s, and an individual heart rate adapted pitch ranging from 0.15–0.28. Tube voltages A and B were 90 kV and Sn150 kV, respectively. The scanning time was 3.59–7.72 s. For contrast enhancement, iohexol (350 mg I/ml) was administered using a 24G needle access in an ear vein. A dual-phase injection protocol was used to administer 20–25 ml of contrast material at a flow rate of 2–2.5 ml/s, followed by injection with 20–25 ml of a mixture of contrast medium and normal saline at a concentration ratio of 1: 1 and a flow rate of 2–2.5 ml/s. The scan delay was determined using the bolus tracking technique. The scanning range was set between the levels of the aortic root and the diaphragmatic surface of the heart. The data acquisition commenced 5 s after a threshold of 100 Hounsfield units (HU), which was maintained in a region of interest (ROI) positioned in the ascending aorta. Depending on the heart rate, the volume CT dose index (CTDIvol) ranged from 22.35–49.22 mGy. The mean heart rate

during third-generation DSCT scanning was 68 ± 19 beats per minute (bpm) (range, 39–102 bpm).

DSCT imaging processing procedures

All datasets were transferred to an off-line syngo.via workstation for further analysis (Siemens Healthcare, Forchheim, Germany). The data were reconstructed by the Bv40 vascular algorithm for every 5% (0–95%) of the R-R interval and with a 1.5 mm slice width (with 1.0 mm increments). After reconstruction at the main station, these data were transferred to the workstation for cardiac function analysis by syngo.via software (Siemens Healthcare, Forchheim, Germany) to observe the end-systolic and end-diastolic image phases. By manual initialization, the mitral valve plane was edited, and the LV endocardial and epicardial contours were delineated. Finally, a quantitative index of global cardiac function and a bull's-eye map with LV myocardial segmentation were obtained.

DSCT imaging data analysis

DSCT images were assessed using a double-blind strategy by two attending physicians with more than five years of experience in cardiac image interpretation. For the quantitative assessment, end-systolic and end-diastolic images from the base to the apex of the LV were used, with end-systole defined as the maximum contraction and end-diastole defined as the maximum dilatation of the LV. Papillary muscles were included in the ventricular lumen. The American Heart Association (AHA)

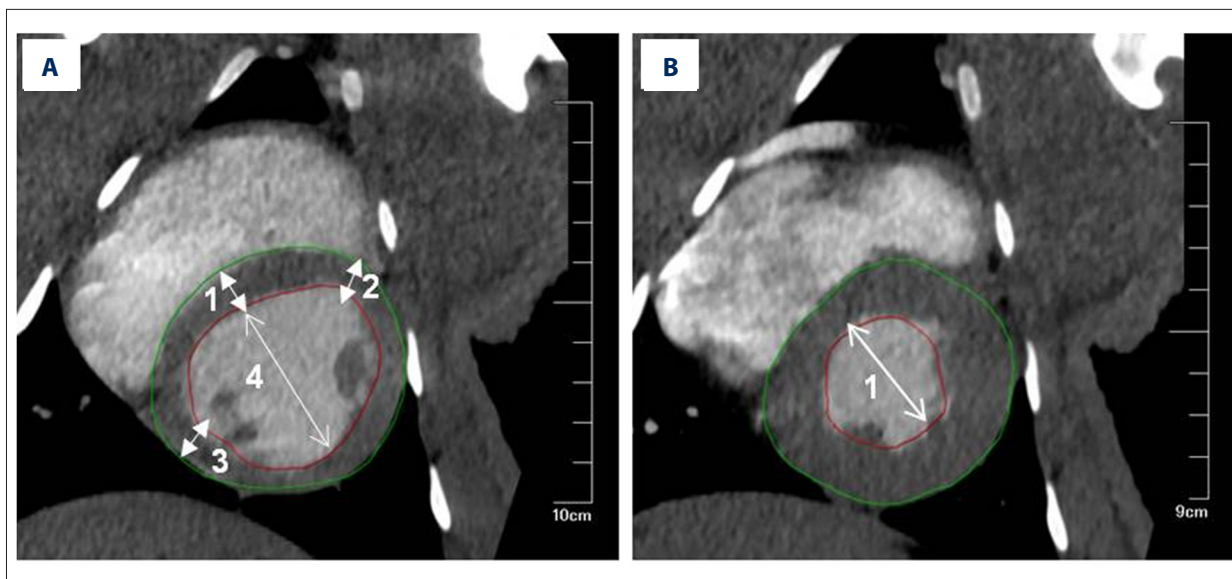


Figure 2. Representative images showing the measurements for the left ventricle (LV) structural parameters. (A) (1) Interventricular septum (IVS) thickness. (2) Left ventricular anterior wall (LVAW) thickness. (3) Left ventricular posterior wall (LVPW) thickness. (4) Left ventricular end-diastolic (LVED) diameter. (B) (1) Left ventricular end-systolic (LVES) diameter.

2002 Heart Standard Plane Nomenclature [23] was used for the determination of the following parameters. Interventricular septum (IVS) thickness: avoiding the LV outflow tract level, showing a complete circle in the LV short-axis position at the end of diastole in the basal segment LV muscle, with measurements performed perpendicular to the endocardium. Left ventricular anterior wall (LVAW) thickness: endocardial measurements were performed at the end of diastole with the IVS in the same plane, perpendicular to the anterior wall of the LV. Left ventricular posterior wall (LVPW) thickness: endocardial measurements were performed at the end of diastole with the IVS in the same plane, perpendicular to the posterior wall of the LV. Left ventricular end-diastolic diameter (LVEDD): at the end of diastole, the LV was measured in the same plane as the IVS and LVPW. Left ventricular end-systolic diameter (LVESD): at the end of systole, the LV diameter was measured in the same plane as the IVS and LVPW (Figure 2). The left ventricular ejection fraction (LVEF), left ventricular end-diastolic volume (LVEDV), left ventricular end-systolic volume (LVESV), stroke volume (SV), LV ejection fraction (LVEF), cardiac output (CO), and end-diastolic LV mass were calculated automatically by computer according to the modified Simpson's method [18].

Statistical analysis

Data were analyzed using SPSS version 22.0 statistical software (SPSS, Inc., Chicago, IL, USA). After confirmation of the normality of distribution using Shapiro-Wilk's test, continuous parameters were presented as the mean±standard deviation (SD) and compared with a two-tailed independent sample t-test. For parameters repeatedly measured at more than

Table 1. Left ventricular structure and global functional parameter baseline measurement result (n=14).

	Mean	Standard deviation (SD)
IVS (mm)	8.50	±0.90
LVAW (mm)	8.40	±1.30
LVPW (mm)	7.80	±1.20
LVED (mm)	45.00	±4.90
LVES (mm)	25.90	±4.10
LVEDV (ml)	74.62	±13.54
LVESV (ml)	23.06	±7.46
LVEF (%)	69.29	±6.83
LV mass (g)	86.35	±14.02
SV (ml)	51.56	±9.77
CO (l/min)	4.22	±2.14

IVS – interventricular septum; LVAW – left ventricular anterior wall; LVPW – left ventricular posterior wall; LVEDD – left ventricular end-diastolic dimension; LVESD – left ventricular end-systolic dimension; LVEDV – left ventricular end-diastolic volume; LVESV – left ventricular end-systolic volume; LVEF – left ventricular ejection fraction; LV mass – left ventricular mass; SV – stroke volume; CO – cardiac output.

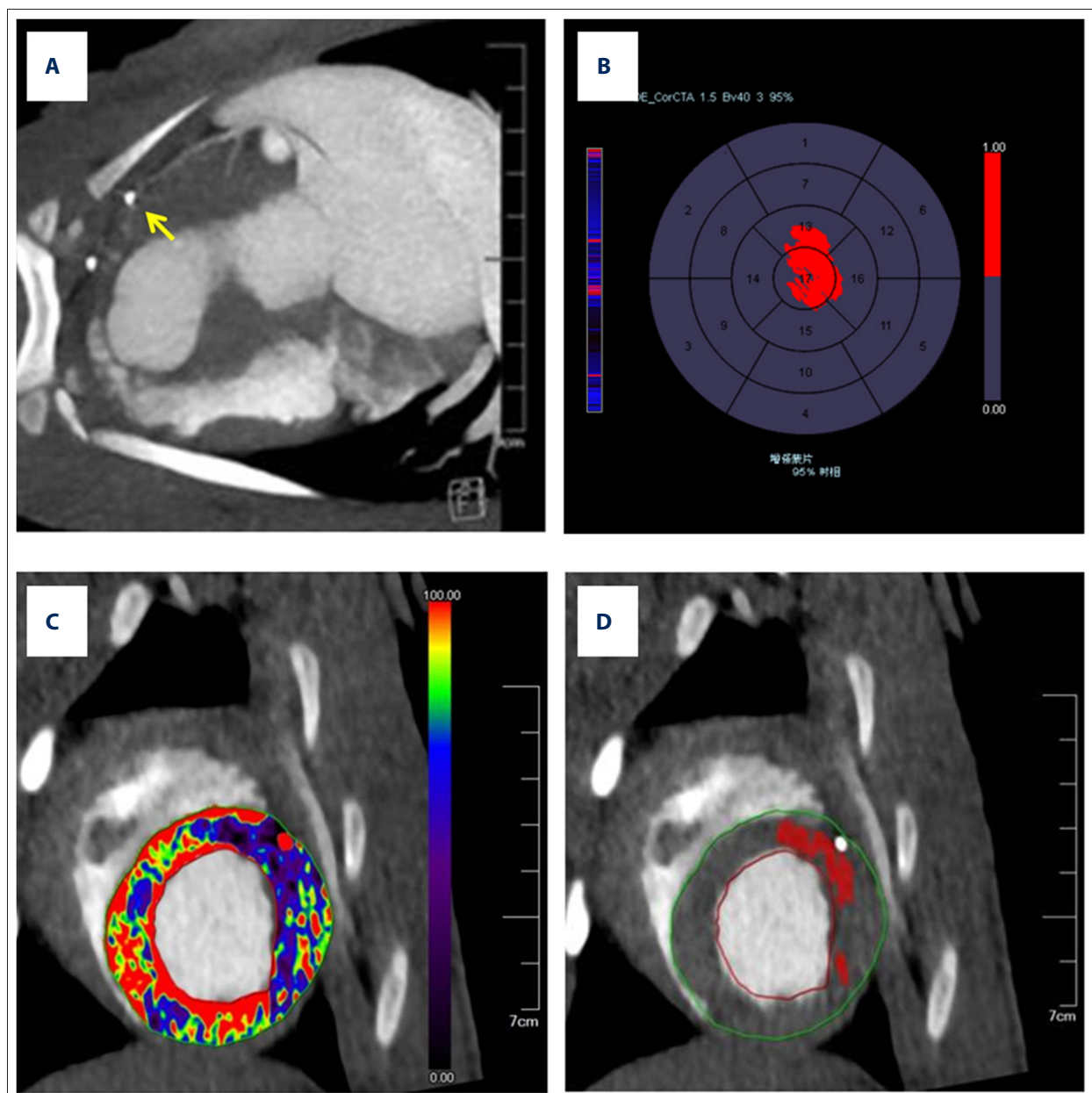
two timepoints, the one-way repeated measures analysis of variance (RM-ANOVA) was used. A P-value <0.05 was considered statistically significant.

Results

The 14 Diannan small-ear pigs in this study underwent examination by third-generation dual-source computed tomography (DSCT) before the induction of acute myocardial infarction (AMI). The baseline left ventricle (LV) structural parameters, including the left ventricular anterior wall (LVAW) thickness, the left ventricular posterior wall (LVPW) thickness, the LV end-diastolic dimension (LVEDD), and LV end-systolic dimension (LVESD), as well as the LV functional parameters, including the LV end-diastolic volume (LVEDV), the LV end-systolic volume (LVESV), the left ventricle ejection fraction (LVEF), the LV mass, stroke volume (SV), and cardiac output (CO) are shown in Table 1.

Among the eight pigs in which AMI was induced, two pigs died, one from ventricular fibrillation after 20 minutes of coronary occlusion, and another from a reaction to the anesthesia, two hours after the operation. The remaining six pigs survived the procedure, and the AMI model was successfully established. Computed tomography angiography (CTA) and first-pass perfusion confirmed the successful preparation of the model (Figure 3), with a success rate of 75%. There were 12 pigs, six in the control group, and six in the AMI group, that underwent serial third-generation DSCT examination after the operation.

The dynamic changes in LVESV, LVEF, SV, and CO are shown in Figure 4. The results confirmed that time affected the LVESV,



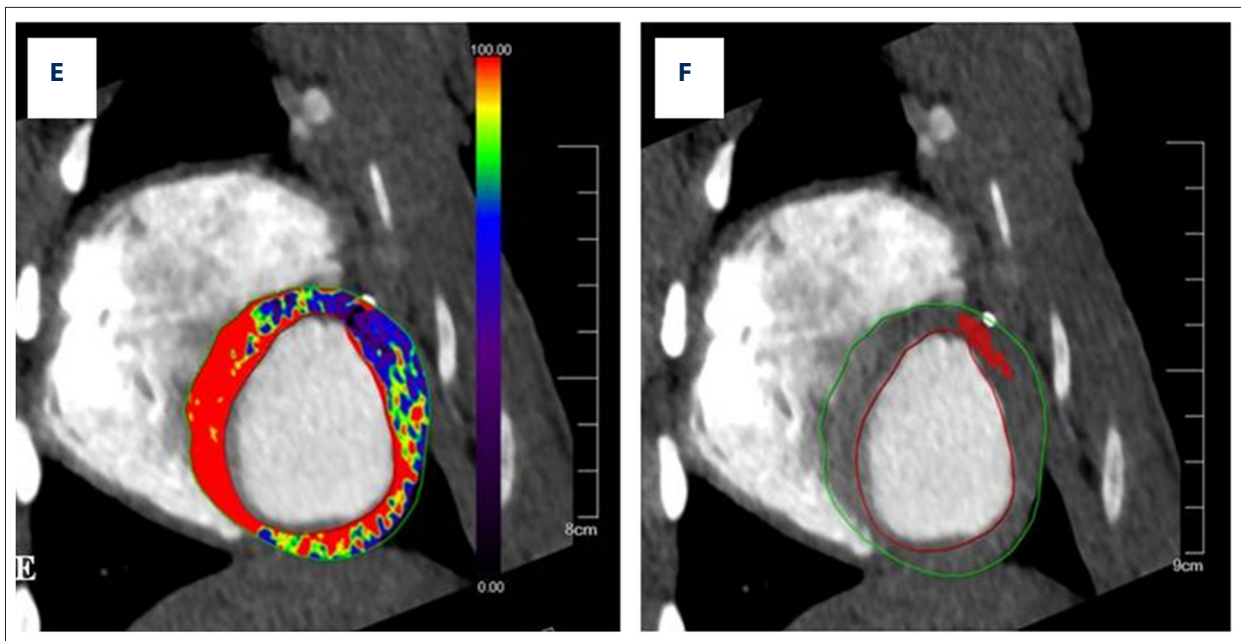


Figure 3. Representative images for the third-generation dual-source computed tomography (DSCT) measurements. (A) Computed tomography angiography (CTA) imaging confirmed the successful preparation of the model and show that the distal end of the left anterior descending (LAD) coronary artery is occluded. The position of the balloon is visible. (B) The enhanced image shows that the left ventricle (LV) apex and the anterior apical segment are significantly affected. (C, D) First-pass perfusion images of the LV end-systolic short-axis position show significant perfusion defects in the affected segments. (E, F) First-pass perfusion images of the LV end-diastolic short-axis position showed significant perfusion defects in the affected segments.

LVEF, SV, and CO ($P < 0.05$), and these four parameters showed significant differences between the two groups ($P < 0.05$). Specifically, from a baseline value of $69.83 \pm 6.09\%$, the LVEF decreased to $50.33 \pm 5.66\%$ at 30 days after AMI. The SV decreased from 53.07 ± 6.51 ml to 40.85 ± 4.97 ml at 30 days after AMI, while the LVESV increased from 22.97 ± 4.55 ml to 40.71 ± 6.42 ml, and the CO decreased from 5.06 ± 2.42 l/min to 3.82 ± 1.69 l/min at 30 days after AMI. These changes were most significant at one hour after the establishment of the AMI model, peaked at six hours after AMI, and then showed a trend of gradual recovery (Figure 4). Time was not shown to be an influencing factor for LVEDV or LV mass ($P > 0.05$), but significant differences in the LVEDV and LV mass were observed between the two study groups ($P < 0.05$) (Figure 5).

Discussion

In this study, baseline data for left ventricle (LV) structure and global LV function in a Diannan small-ear pig model of acute myocardial infarction (AMI) were obtained using third-generation dual-source computed tomography (DSCT) imaging. The results from the dynamic changes in global LV functional parameters using third-generation DSCT in this porcine model of AMI may help to provide basic data and references for CT evaluation in preclinical studies of AMI in miniature pigs.

In this pilot study, third-generation DSCT was validated as a tool for the assessment of dynamic changes in LV functional parameters in the porcine model of AMI.

Obtaining accurate baseline values is important for the application of new innovative techniques in both experimental and clinical studies [21]. The findings from the present study showed that the left ventricular end-systolic volume (LVESV) was lower, and the left ventricle ejection fraction (LVEF) and stroke volume (SV) were higher compared with the findings previously reported from studies that used early-generation DSCT [22,24]. However, the findings from the present study were similar to those described by Busch et al. in 2008 in a study that compared dual-source CT with cardiac magnetic resonance imaging (MRI) [25]. These differences may be explained by the increased temporal resolution of third-generation DSCT, which is the reason that this technique is associated with significantly improved accuracy of data due to optimized end-systolic matching when compared with earlier generation CT scanning [26].

However, the average heart rate of experimental animals is relatively rapid, and this study did not use drug treatment to reduce the heart rate of the pigs, which could be a reason for the slight overestimation of the LVEF. Overall, the values of the LV functional indicators were within the reference ranges

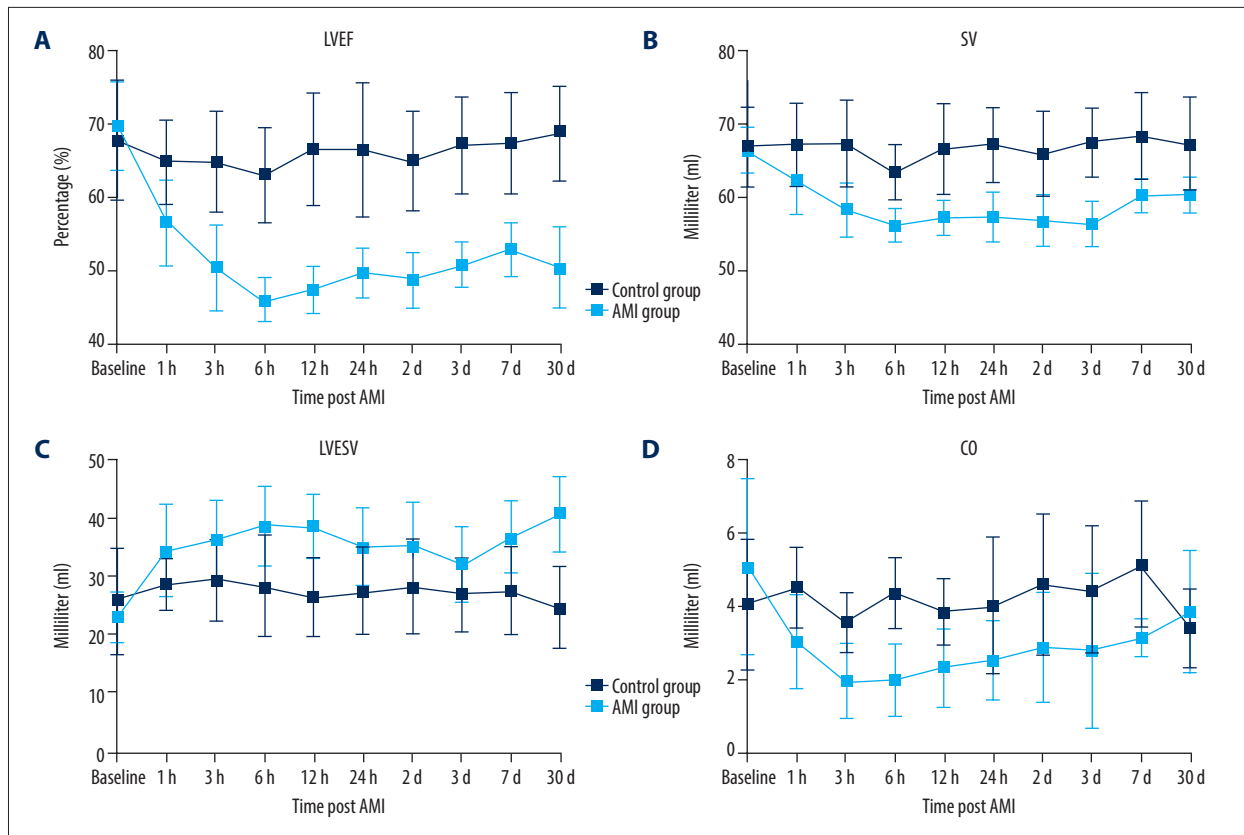


Figure 4. Dynamic changes in left ventricle (LV) functional parameters assessed by serial third-generation dual-source computed tomography (DSCT) in the Diannan small-ear pig model of acute myocardial infarction (AMI). Diannan small-ear pigs in the AMI group (light blue) and the control group (deep blue). **(A)** Left ventricular ejection fraction (LVEF). **(B)** Stroke volume (SV). **(C)** Left ventricular end-systolic volume (LVESV). **(D)** Cardiac output (CO). Data are expressed as the mean \pm standard deviation (SD). * $P < 0.05$ indicates statistical significance.

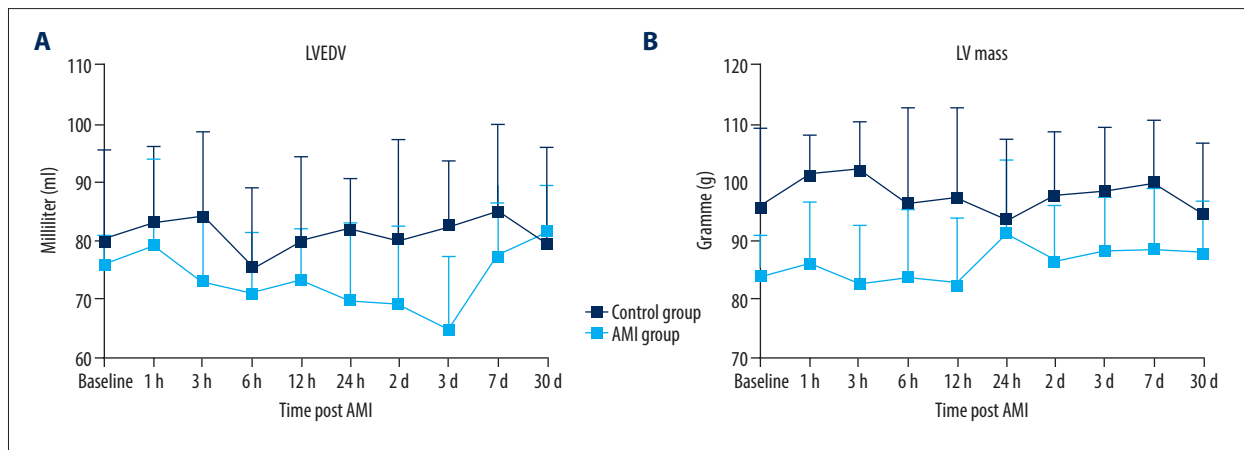


Figure 5. Dynamic changes in the left ventricular end-diastolic volume (LVEDV) and left ventricle (LV) mass assessed by serial third-generation dual-source computed tomography (DSCT) in the Diannan small-ear pig model of acute myocardial infarction (AMI). Diannan small-ear pigs in the AMI group (light blue) and the control group (deep blue). **(A)** Dynamic changes in the LVEDV. Tests of within-subject effects: $F = 1.83$; * $P = 0.07$. Tests of between-subject effects: $F = 6.77$; * $P = 0.02$. **(B)** Dynamic changes in LV mass. Tests of within-subject effects: $F = 0.77$; * $P = 0.64$. Tests of between-subject effects: $F = 16.80$; * $P < 0.05$. LVEDV – left ventricular end-diastolic volume; LV mass – left ventricle mass.

provided by the analysis software, indicating that the values of these indicators were similar to human levels. These results further support that clinically, the third-generation DSCT, or multidetector computed tomography (MDCT) method, offers good agreement with MRI in assessing LV function [14,15]. With a lower radiation dose, high-performance MDCT methods have also become an optimal method for assessing LV function after AMI and ischemia-reperfusion [27–29].

The severity of LV dysfunction after AMI is an important prognostic factor for the development of congestive heart failure (CHF) and sudden cardiac death in patients with AMI [30]. The accurate measurement of LV function after AMI is important for risk stratification of these patients [31]. The findings from this study confirmed that third-generation DSCT could accurately evaluate changes in cardiac function during the hyperacute period after AMI. The changes in LVEF and SV were significant as early as one hour after AMI, as shown in this study.

The results from a previous study showed that systolic function after AMI was an independent predictor of recovery of LVEF. However, because of early-stage percutaneous coronary intervention after AMI, it is difficult to obtain a timeframe for revascularization. Also, there is a lack of information regarding LV function or initial post-hospital revascularization before the index AMI, which prevents an effective prediction of LV recovery [27]. The findings from the present study showed that the dimensions of the LV were significantly increased in the AMI group when compared with the controls, and the absolute magnitude of these differences was not affected by time, demonstrating that LV dilatation occurs rapidly following AMI, which is consistent with previously reported findings [17]. Another important result from the present study was that the peak imaging changes occurred six hours after AMI, and while the change then gradually recovered, the values did not return to the preoperative baseline levels. These findings may provide a basis for correlation analysis between improvement in LV systolic function and revascularization after AMI, which should be investigated in future studies using third-generation DSCT in this animal model and other animal models.

Trends in the changes in LVEDV and LV mass over time were not observed in the present study, which might have been due to several factors. First, AMI caused by complete occlusion is characterized by LV systolic dysfunction. Second, in this study, the post-AMI follow-up period was 30 days, which may not be sufficiently long to reflect changes in LV remodeling. Also, animal models of AMI and ischemia-reperfusion are

mostly prepared using the coronary artery balloon occlusion method [17,19,20,32]. However, the success rate for establishing an AMI model in large animals has been rarely reported. We found that it may be wise to reduce the coronary occlusion if the heart function parameters met the experimental requirements. The intravenous infusion of a bolus of 50 mg lidocaine followed by infusion at a rate of 50 µg/kg/min helps increase the success rate of the establishment of the model. This finding may be related to the preventative effect of lidocaine against ventricular arrhythmia through membrane stabilization and increasing shock-induced thresholds for ventricular fibrillation.

This study had several limitations that should be considered. First, this was a pilot study that included a small study sample size, and the findings require further validation in a larger number of animals to achieve a generalized reference range for LV structural and functional parameters derived by third-generation DSCT. Second, the control group in this study did not include one which was treated with a sham procedure. Third, no quantitative analysis of local LV local function at different stages after AMI was performed to determine trends in the changes of these parameters over time. Fourth, the observation period of 30 days may not be sufficiently long to observe LV remodeling. Finally, this study did not collect hemodynamic data following the induction of AMI in the Diannan small-eared pig model.

Conclusions

In this study, baseline data for left ventricular (LV) structure and global function in miniature pigs were obtained by third-generation dual-source computed tomography (DSCT). These preliminary results validate third-generation DSCT as a useful tool for the assessment of dynamic changes in the LV global functional characteristics in the Diannan small-ear pig model of acute myocardial infarction (AMI).

Acknowledgments

The authors thank Dr. Min Qi from the Radiology Department of the Third People's Hospital of Kunming for her contribution to the experimental study.

Conflict of interest

None.

References:

1. Zhang L, Desai NR, Li J et al: National quality assessment of early clopidogrel therapy in Chinese patients with acute myocardial infarction (AMI) in 2006 and 2011: Insights from the China patient-centered evaluative assessment of cardiac events (PEACE)-retrospective AMI study. *J Am Heart Assoc*, 2015; 4: 1–16
2. Benjamin EJ, Virani SS, Callaway CW et al: Heart disease and stroke statistics – 2018 update: A report from the American Heart Association. *Circulation*, 2018; 137: e492
3. Han R, Sun K, Lu B et al: Diagnostic accuracy of coronary CT angiography combined with dual-energy myocardial perfusion imaging for detection of myocardial infarction. *Exp Ther Med*, 2017; 14: 207–13
4. Iannaccone M, Gili S, De Filippo O et al: Diagnostic accuracy of functional, imaging and biochemical tests for patients presenting with chest pain to the emergency department: A systematic review and meta-analysis. *Eur Heart J Acute Cardiovasc Care*, 2019; 8(5): 412–20
5. Bellenger NG, Burgess MI, Ray SG et al: Comparison of left ventricular ejection fraction and volumes in heart failure by echocardiography, radionuclide ventriculography and cardiovascular magnetic resonance; Are they interchangeable? *Eur Heart J*, 2000; 21: 1387–96
6. Dewey M, Muller M, Eddicks S et al: Evaluation of global and regional left ventricular function with 16-slice computed tomography, biplane cineventriculography, and two-dimensional transthoracic echocardiography: Comparison with magnetic resonance imaging. *J Am Coll Cardiol*, 2006; 48: 2034–44
7. Dewey M, Schink T, Dewey CF: Claustrophobia during magnetic resonance imaging: Cohort study in over 55,000 patients. *J Magn Reson Imaging*, 2007; 26: 1322–27
8. Johnson TR, Nikolaou K, Wintersperger BJ et al: Dual-source CT cardiac imaging: initial experience. *Eur Radiol*, 2006; 16: 1409–15
9. Yang X, Gai LY, Li P et al: Diagnostic accuracy of dual-source CT angiography and coronary risk stratification. *Vasc Health Risk Manag*, 2010; 6: 935–41
10. Dewey M, Teige F, Schnapauff D et al: Non-invasive detection of coronary artery stenoses with multislice computed tomography or magnetic resonance imaging. *Ann Intern Med*, 2006; 145(6): 407–15
11. Wu YW, Tadamura E, Yamamuro M et al: Estimation of global and regional cardiac function using 64-slice computed tomography: A comparison study with echocardiography, gated-SPECT and cardiovascular magnetic resonance. *Int J Cardiol*, 2008; 128: 69–76
12. Takx RA, Moscariello A, Schoepf UJ et al: Quantification of left and right ventricular function and myocardial mass: Comparison of low-radiation dose 2nd generation dual-source CT and cardiac MRI. *Eur J Radiol*, 2012; 81: e598–604
13. Srichai MB, Chandarana H, Donnino R et al: Diagnostic accuracy of cardiac computed tomography angiography for myocardial infarction. *World J Radiol*, 2013; 5: 295–303
14. Rigolli M, Anandabaskaran S, Christiansen JP et al: Bias associated with left ventricular quantification by multimodality imaging: A systematic review and meta-analysis. *Open Heart*, 2016; 3: e000388
15. Kaniewska M, Schuetz GM, Willun S et al: Non-invasive evaluation of global and regional left ventricular function using computed tomography and magnetic resonance imaging: a meta-analysis. *Eur Radiol*, 2017; 27: 1640–59
16. Mangold S, Wichmann JL, Schoepf UJ et al: Diagnostic accuracy of coronary CT angiography using 3(rd)-generation dual-source CT and automated tube voltage selection: Clinical application in a non-obese and obese patient population. *Eur Radiol*, 2017; 27: 2298–308
17. Hubbard L, Lipinski J, Ziemer B et al: Comprehensive assessment of coronary artery disease by using first-pass analysis dynamic CT perfusion: Validation in a swine model. *Radiology*, 2018; 286: 93–102
18. Brodoefel H, Reimann A, Klumpp B et al: Sixty-four-slice CT in the assessment of global and regional left ventricular function: comparison with MRI in a porcine model of acute and subacute myocardial infarction. *Eur Radiol*, 2007; 17: 2948–56
19. Schwarz F, Hinkel R, Baloch E et al: Myocardial CT perfusion imaging in a large animal model: Comparison of dynamic versus single-phase acquisitions. *JACC Cardiovasc Imaging*, 2013; 6: 1229–38
20. Whitaker J, Tschabrunn CM, Jang J et al: Cardiac MR characterization of left ventricular remodeling in a swine model of infarct followed by reperfusion. *J Magn Reson Imaging*, 2018; 9: 1–10
21. Huenges K, Pokorny S, Berndt R et al: Transesophageal echocardiography in swine: Establishment of a baseline. *Ultrasound Med Biol*, 2017; 43: 974–80
22. Mahnken AH, Bruners P, Bornikoel CM et al: Dual-source CT assessment of ventricular function in healthy and infarcted myocardium: An animal study. *Eur J Radiol*, 2011; 77: 443–49
23. Cerqueira MD, Weissman NJ, Dilsizian V et al: Standardized myocardial segmentation and nomenclature for tomographic imaging of the heart. A statement for healthcare professionals from the Cardiac Imaging Committee of the Council on Clinical Cardiology of the American Heart Association. *Circulation*, 2002; 105: 539–42
24. Saeed M, Bajwa HZ, Do L et al: Multi-detector CT and MRI of microembolized myocardial infarct: monitoring of left ventricular function, perfusion, and myocardial viability in a swine model. *Acta Radiol*, 2016; 57: 215–24
25. Busch S, Johnson TR, Wintersperger BJ et al: Quantitative assessment of left ventricular function with dual-source CT in comparison to cardiac magnetic resonance imaging: initial findings. *Eur Radiol*, 2008; 18: 570–75
26. Orakzai SH, Orakzai RH, Nasir K et al: Assessment of cardiac function using multidetector row computed tomography. *J Comput Assist Tomogr*, 2006; 30: 555–63
27. Wen Z, Ma H, Zhao Y et al: Left ventricular diastolic dysfunction assessment with dual-source CT. *PLoS One*, 2015; 10: e0127289
28. Kara B, Nayman A, Guler I et al: Quantitative assessment of left ventricular function and myocardial mass: A comparison of coronary CT angiography with cardiac MRI and echocardiography. *Pol J Radiol*, 2016; 81: 95–102
29. Takx RAP, Vliegenthart R, Schoepf UJ et al: Prognostic value of CT-derived left atrial and left ventricular measures in patients with acute chest pain. *Eur J Radiol*, 2017; 86: 163–68
30. Brooks GC, Lee BK, Rao R et al: Predicting persistent left ventricular dysfunction following myocardial infarction: The PREDICTS study. *J Am Coll Cardiol*, 2016; 67: 1186–96
31. Neuschl V, Berecova Z, Madaric J et al: Structural assessment of myocardial infarction scars and left ventricular function with cardiac magnetic resonance imaging in patients at high risk of sudden cardiac death. *Bratisl Lek Listy*, 2018; 119: 259–64
32. Halladin NL, Ekeløf S, Jensen SE et al: Melatonin does not affect oxidative/inflammatory biomarkers in a closed-chest porcine model of acute myocardial infarction. *In Vivo*, 2014; 28: 483–88